AIP | Journal of Applied Physics

Resonant tunneling through double barrier graphene systems: A comparative study of Klein and non-Klein tunneling structures

I. Rodríguez-Vargas, J. Madrigal-Melchor, and O. Oubram

Citation: J. Appl. Phys. **112**, 073711 (2012); doi: 10.1063/1.4757591
View online: http://dx.doi.org/10.1063/1.4757591
View Table of Contents: http://jap.aip.org/resource/1/JAPIAU/v112/i7
Published by the AIP Publishing LLC.

Resonant tunneling through double barrier graphene systems: A comparative study of Klein and non-Klein tunneling structures

I. Rodríguez-Vargas,[1,a)] J. Madrigal-Melchor,[1] and O. Oubram[2]
[1]*Unidad Académica de Física, Universidad Autónoma de Zacatecas, Calzada Solidaridad Esquina Con Paseo La Bufa S/N, 98060 Zacatecas, Zac., Mexico*
[2]*Instituto de Investigaciones en Materiales, Universidad Nacional Autónoma de México, Apartado Postal 70-360, 04510 México D.F., Mexico*

(Received 20 August 2012; accepted 5 September 2012; published online 8 October 2012)

We study the resonant tunneling effects through double barrier graphene systems (DBGSs). We have considered two types of DBGSs in order to take into account or rule out Klein tunneling effects: (1) the well-known and documented electrostatic-barrier structures (EBSs) created by means of electrostatic probes that act perpendicularly to the graphene sheet; and (2) substrate-barrier structures (SBSs) built sitting the graphene layer on alternating substrates, such as SiO_2 and SiC, which are capable of non-open and open an energy bandgap on graphene. The transfer matrix approach is used to obtain the transmittance, linear-regime conductance, and electronic structure for different set of parameters such as electron energy, electron incident angle, barrier, and well widths. Particular attention is paid to the asymmetric characteristics of the DBGSs, as well as to the main differences between Klein and non-Klein tunneling structures. We find that: (1) the transmission properties can be modulated readily changing the energy and angle of the incident electrons, the widths of the well and barrier regions; (2) the linear-regime conductance is easily enhancing, diminishing, and shifted changing from symmetric to asymmetric DBGSs configuration overall in the case of non-Klein tunneling structures; (3) the conductance shows an oscillatory behavior as function of the well width, with peaks that are directly related to the opening and opening-closure of bound-state subbands for EBSs and SBSs, respectively. Finally, it is important to mention that electrostatic DBGSs or substrate DBGSs could be more suitable depending on a specific application, and in the case of non-Klein tunneling structures, they seem possible considering the sophistication of the current epitaxial growth techniques and whenever substrates that open an energy bandgap on graphene, without diminishing the carrier's mobility, be experimentally discovered. © *2012 American Institute of Physics*. [http://dx.doi.org/10.1063/1.4757591]

I. INTRODUCTION

Since the birth of semiconductor quantum structures,[1] resonant tunneling has played a preponderant role to modulate the transmission and transport properties of devices based on these structures.[2] This phenomenon arise when the energy of impinging electrons coincides with the energy of confined states of a quantum structure, typically a quantum well or series of quantum wells.[2] To this respect, new materials with confinement properties, such as graphene,[3] are not the exception.

Graphene[4] a two-dimensional honeycomb lattice of carbon atoms has attracted a lot of attention due to its unusual fundamental properties,[5–13] because it serves as natural bridge between solid state physics and quantum electrodynamics,[14–16] as well as its potential device applications.[17–20] These novel properties-minimum conductivity,[4–6] Klein tunneling,[7–13] and odd-integer-Hall-effect[4,6–8] rely on the gapless linear dispersion relation,[21] $E = \pm\hbar v_F k$, close to the Dirac points as well as the chiral nature of charge carriers in graphene. In particular, Klein tunneling results from suppression of backscattering due to carriers pseudo-spin conservation.[12] This conservation is also manifested in bilayer graphene with the total reflection phenomenon.[12] A key element to test the aforementioned novel effects as well as to understand the transmission and transport properties in graphene-based structures is the physical mechanism to generate potential barriers on graphene. From a theoretical perspective, mechanisms such as electrostatic field,[22–25] magnetic field,[26–30] breaking-symmetry substrates,[31,32] and mechanical deformation[33–35] can be used for that purpose. Some of them preserves the Dirac cone structure,[22–30] supporting Klein tunneling, and others modify the dispersion relation, open a bandgap and even shift the Dirac points,[31–35] ruling out Klein effects. Despite the peculiarities of each case, there is a common factor in all these systems, which is an oscillatory behavior of the transport properties, in particular the linear-regime conductance. Likewise, most of these reports claim that the peaks that show up in the conductance are related to resonant tunneling caused by confined states. Some effort has been undertaken to understand the oscillatory nature of the transport properties of graphene-based structures.[36] However, as far as we can see this study is not conclusive, since the correlation found between the number of conductance peaks and the number of quantum wells that form the structure, which is created by electrostatic probes, does not explain the energy location of the peaks and even more the role played by Klein tunneling. Additionally, it is important to

a)Author to whom correspondence should be addressed. Electronic mail: isaac@fisica.uaz.edu.mx.

highlight that both, bound states and transmission probability depend intrinsically of the transversal wave vector,[3,22] which turns out in a plenty of propagating, bound, and quasi-bound states that can contribute to the transport properties. Most importantly, which of those states correspond to conductance peaks, and what is the reason that makes those states special. From the experimental standpoint, even simple systems such as single electrostatic-barriers, devoted to test Klein tunneling, show conductance oscillations.[37] The authors argue that possibly confinement effects can be responsible for the conductance peaks as result of the finite size of the system.

Within the mentioned context, the present work addresses the main differences between Klein and non-Klein graphene tunneling structures. For this purpose, we have considered two double barrier systems: (1) electrostatic-based barriers that sustain Klein tunneling and (2) substrate-based barriers that rule out Klein tunneling. The transfer matrix method is implemented to analyzed in detail the transmission, transport, and electronic structure for the mentioned structures. The oscillatory nature of the linear-regime conductance and its relation to the spectrum of confined states with and without Klein tunneling contribution is one of the main concerns of the present study. The rest of our work is organized as follows: the electrostatic and substrate double barrier structures as well as the formalism for the calculation of the transmittance, linear-regime conductance, and bound states are described in Sec. II; the numerical results will be presented and discussed in Sec. III; and finally, a conclusion will be given in Sec. IV.

II. METHODOLOGY

In order to obtain the main differences between Klein and non-Klein graphene structures, we have considered simple, versatile, and useful double barrier graphene systems (DBGSs), Fig. 1. These systems allow us to have a simple way to correlate the transport properties with the spectrum of confined states by simply changing from open boundary conditions to hard-wall conditions, or in other words from double barriers to a single quantum well, and in this way avoiding, for example, the intrinsic complexities of multiple-barrier systems.[36] Likewise, among the different mechanisms that can be used to taking into account or rule out Klein tunneling, electrostatic-field and breaking-symmetry-substrate effects are more suitable due to their theoretical simplicity[3,31] as well as their possible experimental realization.[37,38]

In the case of electrostatic structures, an electrostatic field is applied perpendicularly to the graphene sheet, which is typically sitting on non-breaking-symmetry substrate (SiO_2). From a experimental standpoint,[37] this can be achieved through electrostatic probes above (top gate) the graphene sheet and below (back gate) the SiO_2 substrate. The top gate controls the electrostatic-field strength (V_0) and the width on which it acts, whilst the back gate (together with the substrate doping) manage the Fermi energy of the impinging electrons on the barrier, for further details about the experimental setup see Ref. 37. The main effect of the electrostatic potential is a shifting of the Dirac cones proportional to the field strenght V_0. This shiftting can be obtained through the massless Dirac equation,

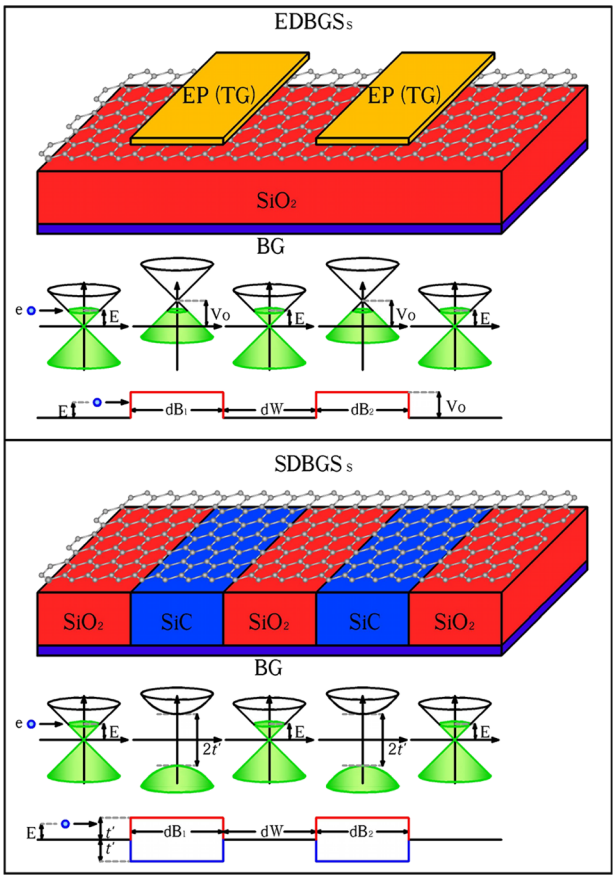

FIG. 1. Schematic representation of the cross-section, dispersion-relation distribution, and energetic representation of (Top) EDBGSs and (Bottom) SDBGSs. EDBGSs are obtained placing two electrostatic probes (EP) or top gates (TG) upon the graphene sheet, which at the same time is sitting on SiO_2 substrate (red slab), turning out in a shifting of the Dirac cones and generating the energy band profile depicted in the third row of top part. For SDBGSs, the graphene layer is placed on an alternating substrate with regions of SiO_2 (red slabs) and SiC (blue slabs), resulting in regions with gapless and gapped linear and parabolic dispersion relations, respectively. For both structures, there is a back gate (BG) that can be used to tune the Fermi level (upper edge of green regions), together with the corresponding n- or p-type doping of the substrates. The difference between vertexes of Dirac cones in EDBGSs, and Dirac cones and Dirac paraboloids in SDBGSs indicates the height of the energy barrier. The blue circle depicts a Dirac electron at the Fermi energy.

$$[v_F(\sigma \cdot p) + V(x)]\psi(x,y) = E\psi(x,y), \tag{1}$$

where the components of pseudospin $\sigma = (\sigma_x, \sigma_y)$ are Pauli matrices, $p = (p_x, p_y)$ is the in-plane momentum operator, and $V(x) = V_0$ is the one-dimensional potential along the x direction and ψ represents the bispinor function. This equation can be readily solved giving the following dispersion relation,

$$E - V_0 = \pm\hbar v_F q, \tag{2}$$

where v_F is the Fermi velocity of Dirac electrons in graphene ($v_F = c/300$), q is the two-dimensional wave vector, and "±" states electrons and holes, respectively. Here, we change the notation of the wave vector from k to q to

differentiate easily the cases without and with electrostatic field, see Introduction. The corresponding wavefunctions, normalized to the graphene sheet area, can be written as

$$\psi_{\pm}(x,y) = \frac{1}{\sqrt{2}}\begin{pmatrix} 1 \\ v_{\pm} \end{pmatrix} e^{\pm iq_x x + iq_y y}, \tag{3}$$

with

$$v_{\pm} = \frac{\pm q_x + iq_y}{E - V_0}. \tag{4}$$

For the case of substrate structures, it is experimentally reported that SiC substrate breaks the symmetry of the graphene sheet, turning out in a bandgap opening.[38] The substrate not only induces a bandgap but also changes the form of the dispersion relation from linear to parabolic.[31] The Dirac-type equation that describes this system is

$$[v_F(\sigma \cdot p) + t'\sigma_z]\psi(x,y) = E\psi(x,y), \tag{5}$$

where $t' = mv_F^2$ is the mass term and σ_z the z component of the Pauli-matrix vector. As in the case of electrostatic field, this equation can be straightforwardly solved giving the parabolic dispersion relation,

$$E^2 = \hbar^2 v_F^2 q^2 + t'^2, \tag{6}$$

where t' is proportional to the bandgap, $E_g = 2t'$. The bandgap can be controlled by the number of graphene layers,[38] taking values of 0.26 eV, 0.14 eV, and 0.066 eV for monolayer, bilayer, and trilayer graphene, respectively. From now on, t' will be 0.13 eV since this work deals with monolayer graphene. The associated wavefunctions keep the same mathematical form, as in the case of graphene subjected to electrostatic field, but now the coefficients of the bispinor come as:[31]

$$v_{\pm} = \frac{E - t'}{\pm q_x - iq_y}. \tag{7}$$

Knowing the dispersion relations and wavefunctions with and without electrostatic field or breaking-symmetry substrate, it is relatively simple to compute the transmission, transport, and electronic structure properties of systems like ones depicted in Fig. 1. Our double barrier system is composed by left and right semi-infinite regions that enclosed two barriers of width d_{B1} and d_{B2} separated by a interwell region of width d_w. The wave vectors of the barrier regions are the same $q_1 = q_3 = q$, since we consider the same barrier height on both barriers, whilst the wave vectors of the semi-infinite and interwell regions are $q_0 = q_2 = q_4 = k$. Taking into account the conservation of the transversal momentum, $k_y = q_y$, and imposing the continuity condition to the wavefunction in the different interfaces along the longitudinal direction (x coordinate), we can obtain a relation between the coefficients of the forward and backward wavefunctions of the left semi-infinite region (A_0 and B_0) and the forward wavefunction of the right semi-infinite region (A_{N+1} and $B_{N+1} = 0$), through the transfer matrix[39,40] as

$$\begin{pmatrix} A_0 \\ B_0 \end{pmatrix} = M \begin{pmatrix} A_{N+1} \\ 0 \end{pmatrix}, \tag{8}$$

where the transfer matrix M is given by,

$$M = D_0^{-1}\left(\prod_{j=1}^{N} D_j P_j D_j^{-1}\right) D_0, \tag{9}$$

is defined in terms of the dynamic D_j and propagation P_j matrices,

$$D_j = \begin{pmatrix} 1 & 1 \\ v_{+,j} & v_{-,j} \end{pmatrix}, \tag{10}$$

and

$$P_j = \begin{pmatrix} e^{-iq_{x,j}d_j} & 0 \\ 0 & e^{iq_{x,j}d_j} \end{pmatrix}, \tag{11}$$

here $j = 1, 2, \ldots, N$, which in our case ($N = 3$) represents the first barrier, the interwell region, and the second barrier, respectively; D_0 is the dynamic matrix of the semi-infinite left and right regions, which in our model are the same. Likewise, $q_{x,1} = q_{x,3} = q_x$ is the x-component of the wave vector of the barriers, and $q_{x,2} = k_x$ corresponds to the longitudinal component of the wave vector of the interwell and semi-infinite regions. According to the characteristics of our system turns out that $D_0 = D_2$ and $D_1 = D_3$. With the transfer matrix at hand, we can compute readily the transmittance,

$$T = \left|\frac{A_{N+1}}{A_0}\right| = \frac{1}{|M_{11}|^2}, \tag{12}$$

with M_{11} the (1, 1) element of the transfer matrix M. The linear-regime conductance is obtained through the Landauer-Buttiker formula[41] as

$$G/G_0 = E_F^* \int_{-\pi/2}^{\pi/2} T(E_F^*, \theta)\cos\theta d\theta, \tag{13}$$

where $E_F^* = E_F/E_0$ is the dimensionless Fermi energy with $E_0 = V_0 = t'$, $G_0 = 2e^2 L_y E_0/h^2 v_F$ is the fundamental conductance factor with L_y the width of the system in the transversal y-coordinate, and θ is the angle of the incident electrons with respect to the x-coordinate. Finally, the spectrum of bound states is calculated changing from open boundary conditions to hard-wall boundary conditions, this is, the widths of the first and last barrier of the multiple structure are extended to infinity. Likewise, we have to require a pure imaginary wave vector for the semi-infinite barrier regions, which turns out in a transcendental equation between energy and transversal wave vector of Dirac electrons as,

$$M_{11}^{BS}(E, k_y; q_x \to i\alpha_x) = 0, \tag{14}$$

where q_x is the wave vector along the x-coordinate defined through Eqs. (2) and (6), and M_{11}^{BS} the (1,1) matrix element of

$$M^{BS} = D_1^{-1}\left(\prod_{j=2}^{N-2} D_j P_j D_j^{-1}\right) D_1. \quad (15)$$

Here, the superscript "BS" has been included to differentiate Eq. (15) from Eq. (9) as well as to state that it corresponds to the bound state case.

III. RESULTS AND DISCUSSION

As previously mentioned, the main concern of the present work is to address the paramount differences between Klein and non-Klein tunneling structures. So, we carry out a comparative analysis of the transmission, transport, and electronic structures properties for electrostatic DBGSs (EDBGSs) and substrate DBGSs (SDBGSs). From an energetically standpoint, the main difference between these structures is that EDBGSs only present a potential barrier for electrons, if the polarity of the applied voltages is the same in both barriers, whilst in SDBGS, potential barriers show up for both electrons and holes, see Fig. 1. This energetic asymmetry will be manifested directly in the physical properties. For the moment, we only warn about it, letting the details later on for each case: transmission, transport, and electronic structure.

In Fig. 2, we show the impact of the second barrier width, d_{B2}, on the transmission probability or transmittance as function of the electron energy for (left column) EDBGSs and (right column) SDBGS. The first, second, and third row correspond to d_{B2} of 50a, 100a, and 200a, respectively. Hereafter, "a" will represent the carbon-carbon distance in graphene, which is equal to 1.42 Å. The widths of the first barrier and interwell region were fixed to $d_{B1} = d_w = 50a$. As we can see from this figure, at normal incidence (dotted-dashed-red lines), a perfect transmission is obtained for EDBGSs irrespective of the width of the second barrier, whilst for SDBGSs, the transmittance is very sensitive to d_{B2}. This remarkable difference between these systems comes from the suppression of back-scattering process at normal incidence for EDBGSs, owing to the conservation of pseudospins.[12,42] On the contrary, the transmission probability for SDBGSs is greatly suppressed for low positive and negative electron energy, due to the evanescent character of the wave functions for both electrons and holes in the barriers.[31] For tilted incidence, similarly to SDBGSs at normal incidence, a transmission gap appears for both EDBGSs and SDBGSs, dotted-solid-black lines of Fig. 2. This transmission gap appears in the positive energy range for EDBGSs, meanwhile for SDBGSs appears for the positive and negative energy range, in other words, it is perfectly symmetric with respect to the origin of energies. Other important characteristic is the acute peaks or transmission window,[36] in the low energy range, associated to the resonant tunneling through DBGSs. The transmission window, small red spots in the low energy range, is perfectly formed for the symmetric case, $d_{B1} = d_w = d_{B2} = 50a$, diminishing and practically disappearing as the width of the second barrier increases

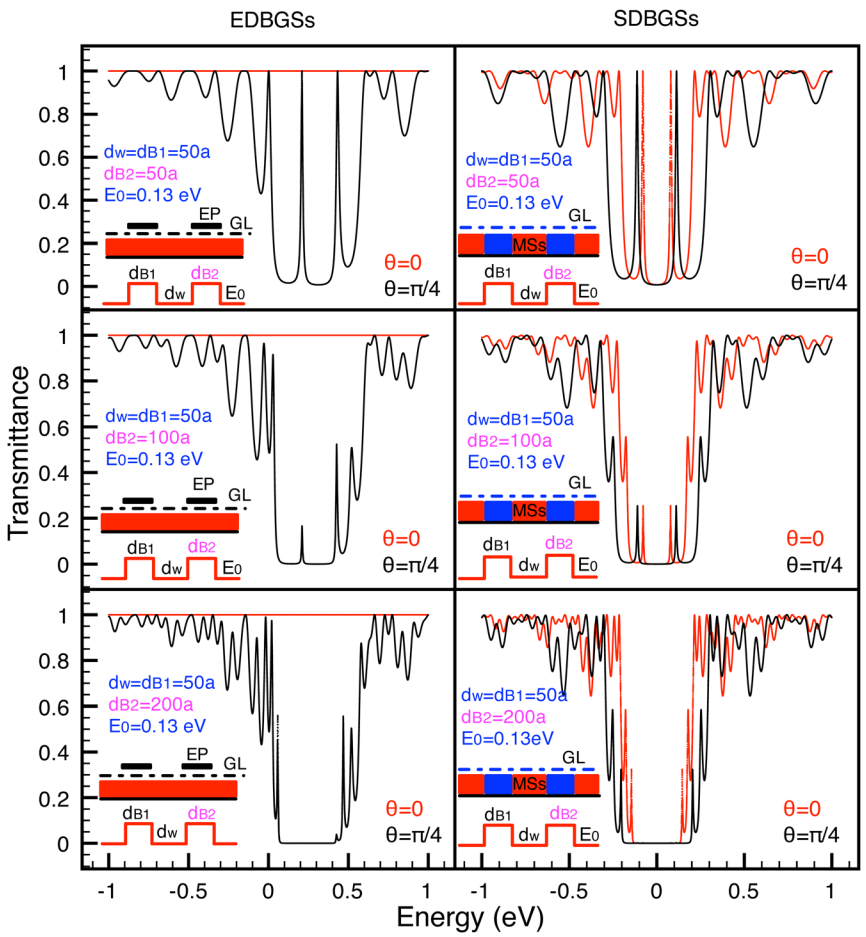

FIG. 2. Comparison of the transmittance as function of energy for (left column) EDBGSs and (right column) SDBGSs. The width of the first barrier and the quantum-well region is fixed to 50a, meanwhile the widths of the second barrier considered are: (first row) 50a, (second row) 100a, and (third row) 200a, respectively. The dotted-dash (red) and dotted-solid (black) lines correspond to normal incidence and incidence at $\pi/4$. The labels in magenta indicate the second barrier width and $E_0 = 0.13$ eV represent the energy barrier height. A schematic representation of the cross-section as well as the potential energy profile are also depicted for both EDBGSs and SDBGSs, insets.

($d_{B2} = 100$a and $d_{B2} = 200$a), due to the exponential dependence of the transmission probability with respect to the barrier width, $e^{-\alpha_x d_{B2}}$. To this respect, the electron will be fully reflected as $d_{B2} \to \infty$, which is the case of total reflection presented in potential steps.[42] In our case, the oblique angle chosen warranty that for a certain energy range, gap region, the evanescent character of waves dominates manifesting in a reduced transmission probability as the second barrier width increases. Additionally, it is important to mention the blue shift of the peaks that form the transmission window as the incidence is tilted for SDBGSs, difference between dotted-solid-black and dotted-dashed-red lines.

The dependence of the transmittance with respect to the quantum well width, d_w, is shown in Fig. 3. The left and right column correspond to EDBGSs and SDBGSs, respectively, the first and second row to quantum well widths of 100a and 200a, and the dotted-dashed-red and dotted-solid-black lines to normal and tilted incidence. At normal incidence, $\theta = 0$, EDBGSs are completely transparent no matter how large the quantum well width is, dotted-dashed-red lines in the left column of Fig. 3. On the contrary, SDBGSs present a little transmission window at normal incidence, dotted-dashed-red lines in the right column of Fig. 3. As the quantum well width doubles its size, the number of acute peaks does in the transmission window, going from two ($d_w = 50a$) to four ($d_w = 100a$) and from four ($d_w = 100a$) to eigth ($d_w = 200a$), see first row and left column of Fig. 2, and left column of Fig. 3. Likewise, we can readily note that the quantum well width determines the location and size of the transmission window.[36] To this respect, the tilted incidence also changes the location and width of the transmission window for both EDBGSs and SDBGSs, blue shifting (in absolute value) the acute peaks that form the transmission window and consequently increasing the width of it. It is also interesting that for large quantum well widths, $d_w = 200a$, the tilted transmission spectra for EDBGSs and SDBGSs show a great similarity, being the main difference the energy shift. This similarity is related to multiple interference effects, since the quantum well region serves as a resonant cavity which perfectly fits the resonant condition as its size is doubled.[42] Even for well widths of 100a and 50a, the similarity shows up in the low energy range.

The angular distribution of the transmission probability is shown in Fig. 4. As in the preceding figures, the left and right panels correspond to EDBGSs and SDBGSs, and the first and second row to the evolution of the transmittance with respect to the second barrier and quantum well width, respectively. The solid-black, dotted-blue, and dashed red lines correspond to: (first row) second barrier width of 50a, 100a, and 200a; (second row) quantum well width of 50a, 100a, and 200a. The energy of the impinging electrons was fixed to $E_i = 0.06$ eV as well as the first barrier and quantum well (second barrier) width, $d_{B1} = d_w = 50$a ($d_{B1} = d_{B2} = 50$a), for the case of the evolution of the transmittance with respect to the second barrier (quantum well) width. The angle is normalized to $\theta_0 = \pi/2$. As we can see for EDBGSs, Klein tunneling manifests clearly at normal incidence irrespective of the second barrier and quantum well widths, even more the transmittance remains practically unchanged up to barrier and well widths of 100a showing a broadening for 200a, with two little peaks for $d_w = 200$a. All this is related to the propagating character of the incident electrons when their energy is below half of the potential barrier height,[42] as in this case $E_i = 0.06$ eV. Likewise, in all cases as the angle of incidence increases, approaching to perpendicular incidence, the transmission probability goes to zero as well. For SDBGSs turn out that the transmittance diminishes drastically as the second barrier width increases, and it is practically negligible with respect to the transmittance of EDBGSs, see first row and second column of Fig. 4.

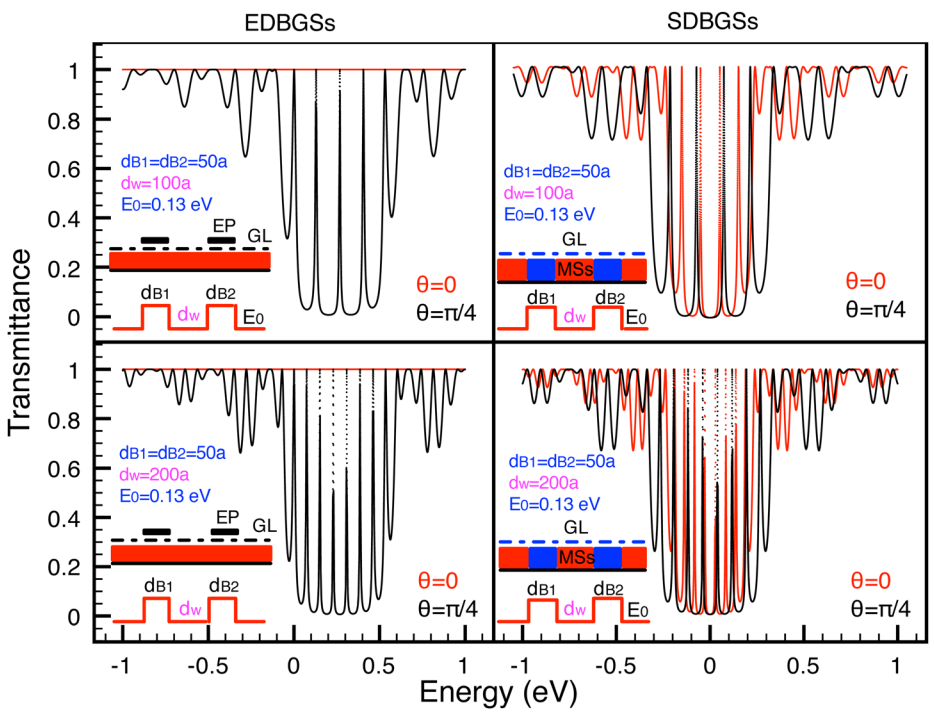

FIG. 3. Same as Fig. 2 but now the first and second barriers are fixed to 50a, meanwhile the quantum-well region is varied: (first row) 100a and (second row) 200a.

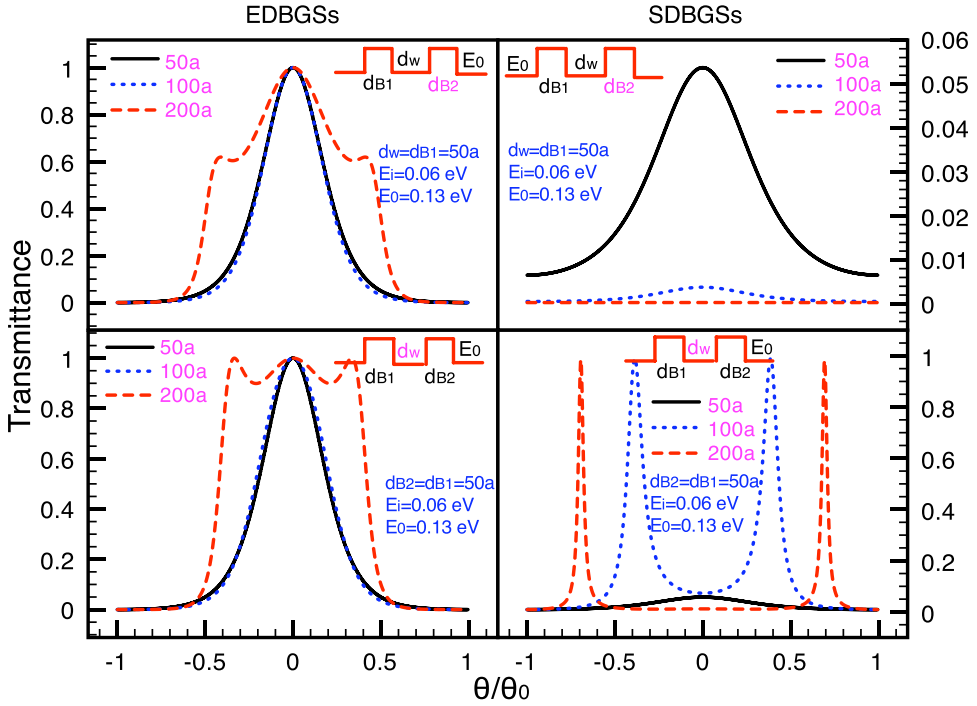

FIG. 4. Angular distribution of the transmittance for (left column) EDBGSs and (right column) SDBGSs. (First row) The width of the first barrier and the quantum-well region is fixed to 50a, meanwhile the widths of the second barrier considered are: (solid-black line) 50a, (dotted-blue line) 100a, and (dashed-red line) 200a, respectively. (Second row) The width of the first and second barrier is fixed to 50a, meanwhile the widths of the quantum-well region considered are: (solid-black line) 50a, (dotted-blue line) 100a, and (dashed-red line) 200a, respectively. The energy of the impinging electron as well as the energy of the potential barrier considered is $E_i = 0.06\,\text{eV}$ and $E_0 = 0.13\,\text{eV}$. The angle is normalized to $\theta_0 = \pi/2$. The labels in magenta indicate the parameter that is varied. A schematic representation of the potential energy profile is also depicted for both EDBGSs and SDBGSs.

This trend comes from the evanescent character of the incident electrons on SDBGSs, no matter if their energy is below or above of half of the potential barrier height. Interesting to note are the resonances that arise as the quantum well width increases, dotted-blue ($d_w = 100$a) and dashed-red ($d_w = 200$a) lines showed in the second row and column of Fig. 4. These resonances are related to the bound states of SDBGSs in the case of hard-wall boundary conditions, or quasi-bound states in this case of open boundary conditions. To complete our discussion of the angular distribution of the transmission probability, we consider incident electrons with energies above $E_0/2$ and below E_0, to be specific $E_i = 0.1\,\text{eV}$, see Fig. 5. For this case, it is well known that electrostatic-barrier structure (EBSs) present the collimation effect or preference for nearly normal incidence.[42] This effect is enhanced as the second barrier width is increased, whilst it is worsen as the quantum well width increases, even more, some resonances associated to bound states appear for tilted incidence far from normal incidence, see left panel of Fig. 5. For SDBGSs, the collimation effect is not present, on the contrary some resonances arise close to $\pi/4$, which slump as the second barrier width increases with negligible transmission probability for $d_{B2} = 200$a. Additionally, as the quantum well width increases the resonances shift to higher

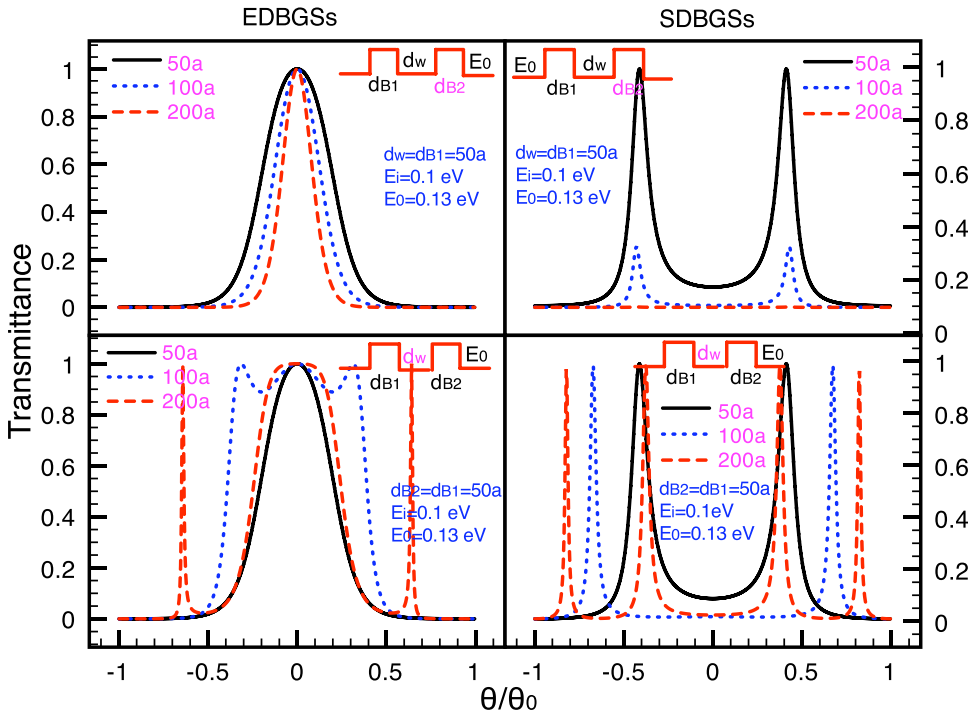

FIG. 5. The same as Fig. 4, but $E_i = 0.1\,\text{eV}$.

energies (dotted-blue) and eventually more than one resonance arise for electrons and holes, see second row and column of Fig. 5.

To have a whole picture of transmittance as function of energy and angle of incidence, (E,θ) contour plots of it are shown in Figs. 6 and 7. The energy and angle of incidence are normalized to $E_0 = 0.13\,\text{eV}$ and $\theta_0 = \pi/2$, respectively. Particularly, Fig. 6 correspond to the evolution of the transmission probability with respect to the second barrier width for (left panel) SDBGSs and (right panel) EDBGSs, whilst Fig. 7 shows the evolution for different quantum well widths, with same correspondence for left and right panels as Fig. 6. From this perspective, we can see the big difference between the transmission properties of EDBGSs and SDBGSs. From one side, SDBGSs show symmetric transmission contours between electrons (positive energy) and holes (negative energy), as well as alternating transmission regions of high and low transmittance of semi-circular shape. For the symmetric structure, $d_{B1} = d_w = d_{B2}$, we can see a transmission window in the low energy range surrounded by very low transmittance regions, this window narrows as the width of the second barrier increases ($d_{B2} = 100$a), being negligible for $d_{B2} = 200$a. From the other side, EDBGSs present a very different transmission contours, in which we can see clearly perfect transmission in the whole energy range for normal incidence and small angles of incidence, irrespective of the second barrier width, as result of Klein tunneling and collimation effect.[42] It is also evident how the second barrier enhances the collimation effect as it increases (low energy range for electrons), as well as redistributes transmission characteristics for holes, even when no barrier is present for them. In Fig. 7, we can see readily the impact of the quantum well width on the transmission properties of DBGSs. First and second row correspond to quantum well widths of 100a and 200a, respectively. For large well widths, transmittance shows a richer structure of transmission windows in the low energy range for both SDBGSs and EDBGSs. Theses resonances can affect importantly the transport properties, linear-regime conductance, of DBGSs as we will see later. Contrary to Fig. 6, the collimation effect remains practically the same, no matter how large the quantum well is.

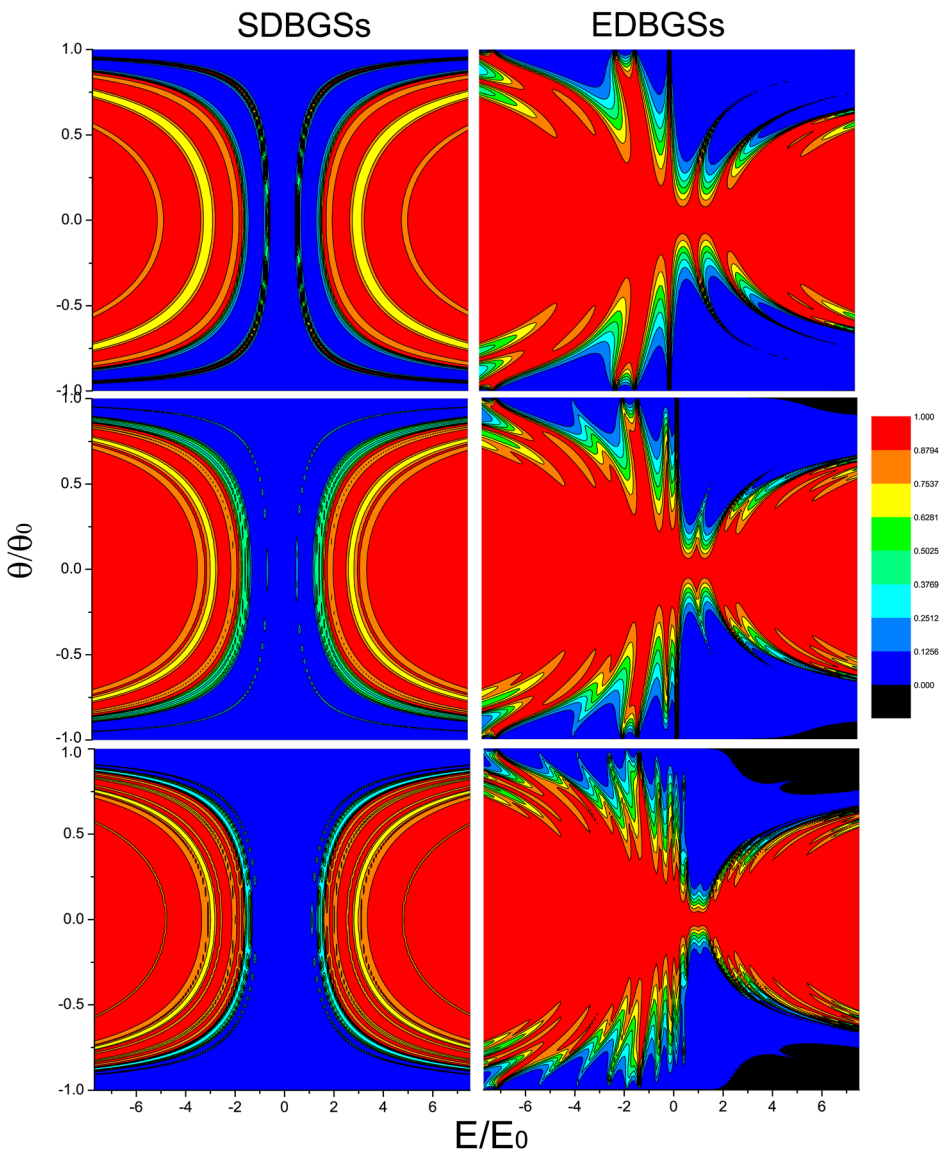

FIG. 6. Contour plot of the electron transmission through (left panel) EDBGSs and (right panel) SDBGSs for interbarrier separation d_{B2} of (first row) 50a, (second row) 100a, and (third row) 200a. The quantum-well region, interbarrier separation of the first barrier, and the energy barrier height are $d_w = d_{B1} = 50$a and $E_0 = 0.13\,\text{eV}$.

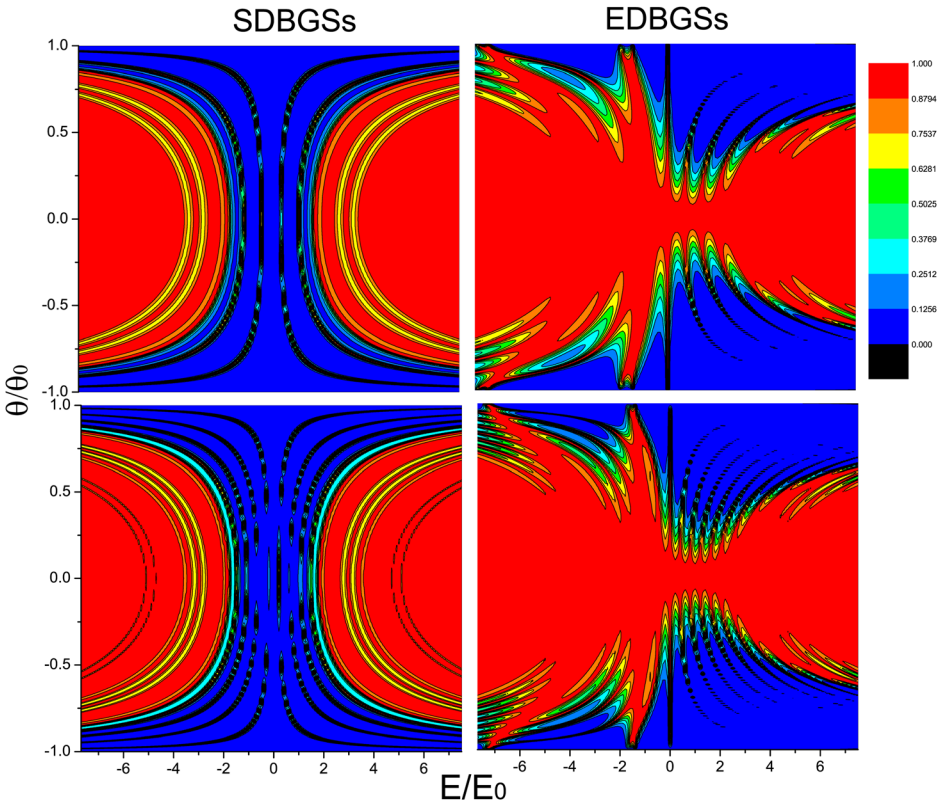

FIG. 7. Contour plot of the electron transmission through (left panel) EDBGSs and (right panel) SDBGSs for interwell separation d_w of (first row) 100a and (second row) 200a. The interbarrier separation of the first and second barrier and the energy barrier height are $d_{B1} = d_{B2} = 50a$ and $E_0 = 0.13\,\text{eV}$.

Now, it is turn to analyze the linear-regime conductance results. As in all cases presented for transmission probability, we paid attention to the impact of the second barrier and quantum well widths on the transport properties, Fig. 8. The black and blue curves belong to EDBGSs and SDBGSs, respectively. Likewise, solid, dotted and dashed curves indicate second barrier (quantum well) widths of 50a, 100a, and 200a, top (bottom) of Fig. 8. EDBGSs show a smooth and broad peak above the barrier height for the symmetric case, solid-black curve. As the second barrier width increases, asymmetric configuration, this peak shifts to lower energies, approaching to the barrier height for $d_{B2} = 200a$. It is also interesting to note the additional peaks in the low energy range for asymmetric configurations, one peak for $d_{B2} = 100a$ (dotted-black) and two peaks for $d_{B2} = 200a$ (dashed-black). Moreover, for $d_{B2} = 200a$, the low energy peaks dominate over the peak above the barrier. In the case of SDBGSs, there is a peak in the conductance below the barrier for symmetric configuration. This peak presents a red-shift as the second barrier gets larger and diminishes one and three orders of magnitude for second barrier widths of 100a and 200a, see right of Fig. 8, which is a zoom of the

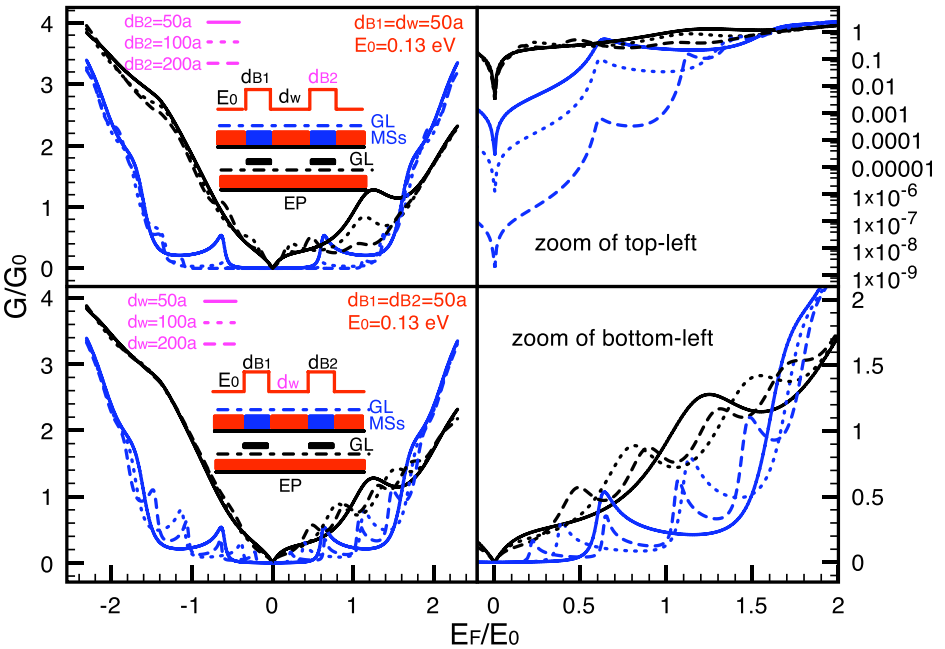

FIG. 8. Conductance through (black lines) EDBGSs and (blue lines) SDBGSs for: (Top) interbarrier separation d_{B2} of (solid line) 50a, (dotted line) 100a, and (dashed line) 200a, respectively; (Bottom) interwell separation d_w of (solid line) 50a, (dotted line) 100a, and (dashed line) 200a. The right panel corresponds to a zoom of the left one.

left part. As we can see, there are no peaks in the low energy range for SDBGSs, contrary to EDBGSs some peaks show up above the barrier. In the bottom of Fig. 8, we can notice the impact of the quantum well width on conductance. Conductance for EDBGSs and SDBGSs show an oscillatory behavior as the quantum well width increases, with one, two and four peaks for $d_w = 50a$, 100a, and 200a, respectively. Apart from the similarities between the transport properties of EDBGSs and SDBGSs, we want to stress three characteristics that differentiate the conductance of these systems: (1) practically in all cases, below $E_F/E_0 = 1.5$, the conductance in EDBGSs is higher than in SDBGSs; (2) there is red shift of conductance peaks for SDBGSs with respect to EDBGSs; (3) a slump is presented for conductance peaks of SDBGSs, which turns out in narrow peaks as compared to EDBGSs.

Aside from multiple reports stressing important effects that can affect the transport properties of graphene-based structures such as defects,[43,44] ripples,[45] vacancies,[9] impurities,[46] and so on, as far as we know, there are no reports addressed to explain the oscillatory nature of conductance in multiple barrier graphene structures. Most of them, mention that the oscillatory behavior of conductance is related to resonances, quasi-bound states, and bound states, irrespective to the mechanism to create the graphene-based structure.[22–35] However, none of them clarify which of the multiple resonances that underlie in these structures are the responsible of the conductance peaks, but even, what determines the differences between the transport characteristics of EDBGSs and SDBGSs. In order to answer these issues, we compute the spectrum of bound states for EDBGSs and SDBGSs, using Eq. (14). Our outcomes are shown in Fig. 9. As we have to impose hard-wall boundary conditions, the different cases presented for second barrier width reduce to one, so strictly speaking, we only consider three cases, which correspond to quantum well widths of 50a, 100a, and 200a, first, second, and third row of Fig. 9. The left panel of Fig. 9 refer to quantum wells created by electrostatic barriers (EQWs), whilst the right panel to quantum wells obtained through barriers created by breaking-symmetry substrates (SQWs). Dashed-red lines delimit the allowed region for bound states. As we can see, there are one, two, and four subbands for EQWs of width d_w, $2d_w$, and $4d_w$, respectively. These subbands, or electron channels, are characterized by a quantum number, as well as the transversal wave vector, and for large values of k_y are given approximately by[3] $E_n(k_y) = \hbar v_F[(n\pi/d_w)^2 + k_y^2]^{1/2}$. We want to highlight that more than electron channels, these subbands represent dispersion branches, and it is well known that when a dispersion channel opens, the transport properties will diminish, with an inverse effect when a dispersion channel closes.[47] These

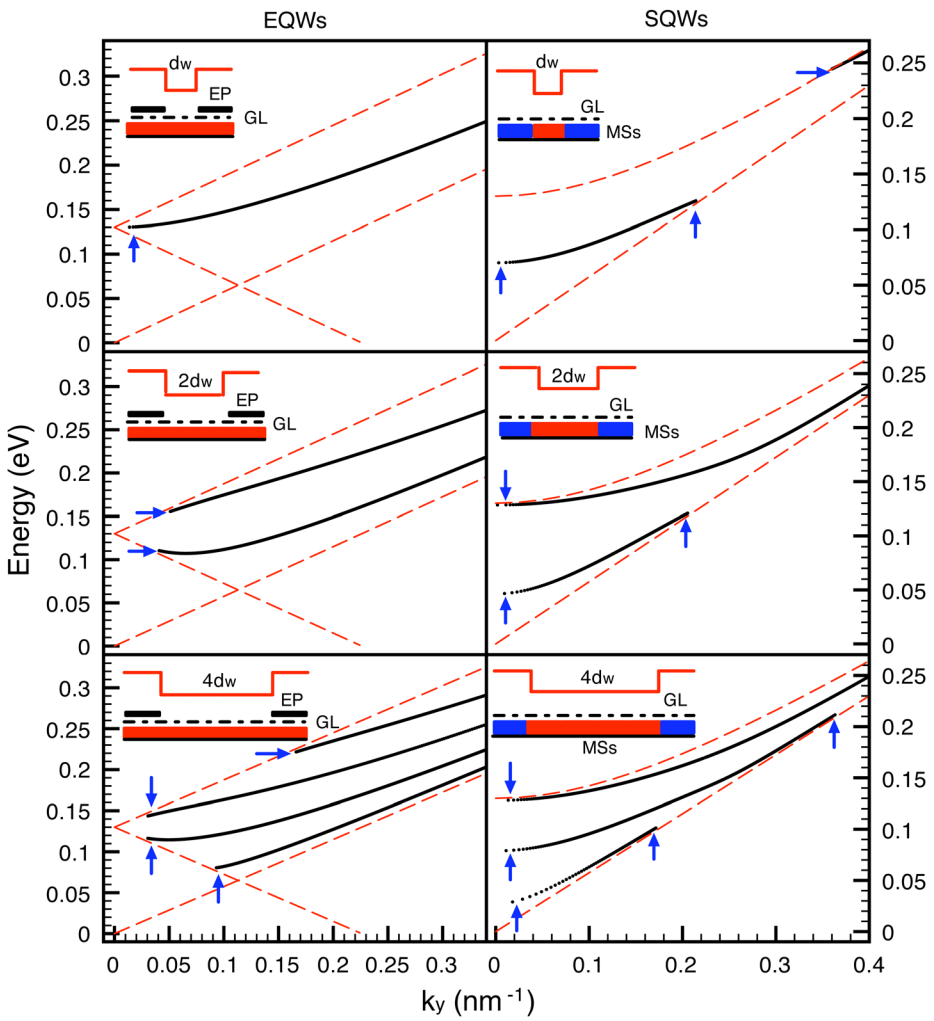

FIG. 9. Spectrum of confined states vs k_y for (left column) EQWs and (right column) SQWs. The first, second, and third row correspond to d_w, $2d_w$, and $4d_w$, with $d_w = 50a$. The blue arrows point out the opening and opening-closure of conduction channels for EQWs and SQWs, respectively.

fundamentals of the transport properties explain quite well, from a qualitative standpoint, the number of conductance peaks for EQWs in each case considered and, from a quantitative perspective, the correspondence between the location of the mentioned peaks and the opening of dispersion channels (blue arrows), even when there is a natural difference between open and hard-wall boundary conditions. Similar arguments apply for SQWs, however in this case, the allowed region for bound states reduces as k_y increases, due to the particular dependence between the quantities that delimit this region, $E^2 = \hbar^2 v_F^2 k_y^2 + t'^2$. As result of this reduction, a systematic closure of dispersion branches is presented, contrary to the systematic opening of electron channels for EQWs. This alternate opening and closure of dispersion channels explains the pronounced increase and reduction in the transport properties, which turns out in acute and narrow conductance peaks as compared to EQWs. Finally, it is important to stress that the conductance peaks in the low energy range for the asymmetric configuration of EDBGSs, dashed-black curve of the top of Fig. 8, are not related to bound states, on the contrary obey a redistribution of transmission probability for propagating states, as we can see from the corresponding contour plot, third row, and second column of Fig. 6.

IV. CONCLUSIONS

In summary, we have studied the transmission, transport, and electronic structure properties of double barrier graphene systems. Particularly, a comparative analysis of Klein and non-Klein graphene structures and electrostatic- and substrate-barrier structures (SBSs) is carried out. The transfer matrix approach has been implemented to obtain the main differences between EDBGSs and SDBGSs. Our results show that the asymmetric configuration of DBGSs readily modulate the transmission and transport properties of both EDBGSs and SDBGSs, as function of the main parameters of the system: well and barrier widths, angle and energy of the incident electrons. Special attention has been paid to the oscillatory nature of the linear-regime conductance, showing that the conductance peaks turn out from the opening and closure of bound-state energy subbands. To this respect, the sharpness of the conductance peaks in SQWs comes from the opening-closure of bound-state energy subbands, meanwhile for EQWs, a systematic opening of subbands as well as Klein tunneling effects turn out in smother conductance peaks and an overall enhancement of the conductance, respectively. Finally, it is important to mention that electrostatic or substrate DBGSs could be more suitable depending on a specific application, and in the case of non-Klein tunneling structures, they seem possible considering the sophistication of the current epitaxial growth techniques and whenever substrates that open an energy bandgap on graphene, without diminishing the carrier's mobility, be experimentally discovered.

ACKNOWLEDGMENT

The authors acknowledge the financial support of CONACyT through Grant CB-2010-151713.

[1]L. Esaki and R. Tsu, IBM J. Res. Develop. **14**, 61 (1970).
[2]R. Tsu and L. Esaki, Appl. Phys. Lett. **22**, 562 (1973); L. L. Chang, L. Esaki and R. Tsu, *ibid.* **24**, 593 (1974).
[3]J. Milton Pereira, Jr., V. Mlinar, F. M. Peeters, and P. Vasilopoulos, Phys. Rev. B **74**, 045424 (2006).
[4]K. S. Novoselov, A. K. Geim, S. V. Mrozov, D. Jiang, Y. Zhang, S. V. Dubonos, I. V. Grigorieva, and A. A. Firsov, Science **306**, 666 (2004).
[5]K. S. Novoselov, A. K. Geim, S. V. Morozov, D. Jiang, M. I. Katsnelson, I. V. Grigorieva, S. V. Dubonos, and A. A. Firsov, Nature **438**, 197 (2005).
[6]\Y. Zhang, Y.-W. Tan, H. L. Stormer, and P. Kim, Nature **438**, 201 (2005).
[7]V. P. Gusynin and S. G. Sharapov, Phys. Rev. Lett. **95**, 146801 (2005).
[8]E. McCann and V. I. Falko, Phys. Rev. Lett. **96**, 086805 (2006).
[9]N. M. R. Peres, F. Guinea, and A. H. Castro Neto, Phys. Rev. B **73**, 125411 (2006).
[10]A. Calogeracos and N. Dombey, Contemp. Phys. **40**, 313 (1999).
[11]C. Itzykson and J.-B. Zuber, *Quantum Field Theory* (Dover, New York, 2006).
[12]M. I. Katsnelson, K. S. Novoselov, and A. K. Geim, Nat. Phys. **2**, 620 (2006).
[13]C. Bai and X. Zhang, Phys. Rev. B **76**, 75430 (2007).
[14]A. H. Castro Neto, F. Guinea, and N. M. R. Peres, Phys. World **19**, 33 (2006).
[15]M. I. Katsnelson, Eur. J. Phys. B **51**, 157 (2006).
[16]M. I. Katsnelson and K. S. Novoselov, Solid State Commun. **143**, 3 (2007).
[17]F. Schedin, A. K. Geim, S. V. Morozov, E. W. Hill, P. Blake, M. I. Katsnelson, and K. S. Novoselov, Nature Mater. **6**, 652 (2007).
[18]A. K. Geim and K. S. Novoselov, Nature Mater. **6**, 183 (2007).
[19]E. W. Hill, A. K. Geim, K. Novoselov, F. Schedin, and P. Blake, IEEE Trans. Magn. **42**, 2694 (2006).
[20]M. Ohishi, M. Shiraishi, R. Nouchi, T. Nozaki, T. Shinjo, and Y. Suzuki, Jpn. J. Appl. Phys., Part 2 **46**, L605 (2007).
[21]P. R. Wallace, Phys. Rev. **71**, 622 (1947).
[22]J. Milton Pereira, Jr., P. Vasilopoulos, and F. M. Peteers, Appl. Phys. Lett. **90**, 132122 (2007).
[23]X. Chen and J.-W. Tao, Appl. Phys. Lett. **94**, 262102 (2009).
[24]J. M. Pereira, Jr., F. M. Peteers, A. Chaves, and G. A. Farias, Semicond. Sci. Technol. **25**, 033002 (2010).
[25]R. Biswas, S. Mukhopadhyay, and C. Sinha, Physica E **42**, 1781 (2010).
[26]A. De Martino, L. Dell'Anna, and R. Egger, Phys. Rev. Lett. **98**, 066802 (2007).
[27]M. Ramezani Masir, P. Vasilopoulos, A. Matulis, and F. M. Peteers, Phys. Rev. B **77**, 235443 (2008).
[28]M. Ramezani, P. Vasilopoulos, and F. M. Peteers, Appl. Phys. Lett. **93**, 242103 (2008).
[29]M. Ramezani, P. Vasilopoulos, and F. M. Peteers, New J. Phys. **11**, 095009 (2009).
[30]M. Ramezani, P. Vasilopoulos, and F. M. Peteers, Phys. Rev. B **82**, 115417 (2010).
[31]J. Viana Gomes and N. M. R. Peres, J. Phys.: Condens. Matter **20**, 325221 (2008).
[32]V. Hung Nguyen, A. Bournel, and P. Dollfus, Semicond. Sci. Technol. **26**, 125012 (2011).
[33]J. Cayssol, B. Huard, and D. Goldhaber-Gordon, Phys. Rev. B **79**, 075428 (2009).
[34]S. Gattenlohner, W. Belzig, and M. Titov, Phys. Rev. B **82**, 155417 (2010).
[35]F. M. D. Pellegrino, G. G. N. Angilella, and R. Pucci, Phys. Rev. B **84**, 195404 (2011).
[36]G. J. Xu, X. G. Xu, B. H. Wu, J. C. Cao, and C. Zhang, J. Appl. Phys. **107**, 123718 (2010).
[37]A. F. Young and P. Kim, Nat. Phys. **5**, 222 (2009).
[38]S. Y. Zhou, G.-H. Gweon, A. V. Fedorov. P. N. First, W. A. de Heer, D.-H. Lee, F. Guinea, A. H. Castro-Neto, and A. Lanzara, Nature Mater. **6**, 770 (2007).
[39]P. Yeh, *Optical Waves in Layered Media* (Wiley-Interscience, 2005).
[40]P. Markos and C. M. Soukoulis, *Wave Propagation: From Electrons to Photonic Crystals and Left-Handed Materials* (Princeton University Press, 2008).
[41]S. Datta, *Electronic Transport in Mesoscopic Systems* (Cambridge University Press, 1995).
[42]P. E. Allain and J. N. Fuchs, Eur. Phys. J. B **83**, 301 (2011).

[43]A. H. Castro Neto, F. Guinea, N. M. R. Peres, K. S. Novoselov, and A. K. Geim, Rev. Mod. Phys. **81**, 109 (2009).
[44]N. M. R. Peres, J. Phys.: Condens. Matter **21**, 323201 (2009).
[45]J. C. Meyer, A. K. Geim, M. I. Katsnelson, K. S. Novoselov, T. J. Booth, and S. Roth, Nature (London) **446**, 60 (2007).
[46]X. Du, I. Skachko, A. Barker, and E. Y. Andrei, Nat. Nanotechnol. **3**, 491 (2008).
[47]V. V. Mitin, V. A. Kochelap, and M. A. Strocio, *Quantum Heterostructures: Microelectronics and optoelectronics* (Cambridge University Press, 1999).